# Comparison of Land–Precipitation Coupling Strength Using Observations and Models

XUBIN ZENG

*Department of Atmospheric Sciences, The University of Arizona, Tucson, Arizona*

MIKE BARLAGE

*Research Applications Laboratory, National Center for Atmospheric Research, Boulder, Colorado*

CHRIS CASTRO

*Department of Atmospheric Sciences, The University of Arizona, Tucson, Arizona*

KELLY FLING

*U.S. Army Aberdeen Test Center, Aberdeen Proving Ground, Maryland*

(Manuscript received 16 October 2009, in final form 24 February 2010)

ABSTRACT

Numerous studies have attempted to address the land–precipitation coupling, but scientists' understanding remains limited and discrepancies still exist from different studies. A new parameter Γ is proposed here to estimate the land–precipitation coupling strength based on the ratio of the covariance between monthly or seasonal precipitation and evaporation anomalies (from their climatological means) over the variance of precipitation anomalies. The Γ value is easy to compute and insensitive to the horizontal scales used; however, it does not provide causality. A relatively high Γ is a necessary—but not sufficient—condition for a relatively strong land–precipitation coupling. A computation of Γ values using two global reanalyses (ECMWF and NCEP), one regional reanalysis [North American Regional Reanalysis (NARR)], and observed precipitation along with Variable Infiltration Capacity (VIC)-derived evaporation data indicates that the land–precipitation coupling is stronger in summer and weaker in winter. The strongest coupling (i.e., hot spots) occurs over the western and central parts of North America, part of the Eurasia midlatitude, and Sahel in boreal summer and over most of Australia, Argentina, and South Africa in austral summer. The Community Climate System Model, version 3 (CCSM3) shows much higher Γ values, consistent with the strong coupling shown by its atmosphere–land coupled components in previous studies. Its overall spatial pattern of Γ values is not affected much over most regions by the doubling of $CO_2$ in CCSM3. The Γ values from the Regional Atmospheric Modeling System (RAMS) are more realistic than those from CCSM3; however, they are still higher than those from observations over North America.

## 1. Introduction

Water is constantly recycled between the atmosphere, biosphere, hydrosphere, and lithosphere, and different processes are responsible for moving water through each component. The fate of a water molecule that is precipitated over land is percolation, runoff, or evapotranspiration *E*, which includes wet canopy evaporation, dry canopy transpiration, and soil evaporation. Less is understood about the fate of water molecules evaporating or transpiring from the surface. In some geographic locations, precipitation *P* may rely heavily on water from local *E*. In other areas, moisture convergence is the dominant source of water for precipitation.

The land surface effect on local precipitation has been studied for more than a century, and early studies were briefly reviewed in Eltahir and Bras (1996). For instance, in the early years of the twentieth century, it was thought that the ratio of surface *E* over *P* would represent the land surface contribution to precipitation over a continent and was estimated to be 70%. This view is incorrect

*Corresponding author address:* Xubin Zeng, Department of Atmospheric Sciences, The University of Arizona, P.O. Box 210081, Tucson, AZ 85721.
E-mail: xubin@atmo.arizona.edu

DOI: 10.1175/2010JHM1226.1

because it was based on a simple and incorrect picture of the water cycle in which the atmospheric moisture inflow to a region, rather than the moisture convergence, is equal to runoff and hence recycled precipitation is equivalent to $E$ (Eltahir and Bras 1996).

This issue has also been studied using isotope data. Isotopes of water depend on the temperature and history of the water, and the analysis of the isotope data in rainfall provides information about the origin of the water molecules. In general, condensation depletes heavy isotope contents in rainfall as the air moves from ocean to land. Therefore, a small isotope gradient from ocean to continental interior might indicate a relatively large contribution of land surface $E$ to $P$. While the isotope data are useful qualitatively, using them to quantify the land surface effect on local precipitation has large uncertainties because of the variability in isotope content of the moisture that contributes to the observed precipitation over a region (Kurita et al. 2004).

Using the precipitation recycling ratio to quantify the contribution of local $E$ to local precipitation has been a popular approach in the past few decades (e.g., Anderson et al. 2008; Bisselink and Dolman 2008). In this approach, the total precipitation in a region is divided into two components: precipitation from moisture advection $P_A$ and that from surface evapotranspiration $P_E$. The recycling ratio $P_E/P$ provides a diagnostic measure of the land surface contribution to local precipitation without explaining the underlying physics (e.g., Brubaker et al. 1993). Different methods have been developed to compute the recycling ratio, usually based on two assumptions: (i) the atmosphere is well mixed, both horizontally and vertically; and (ii) any changes in precipitable water (i.e., vertically integrated water vapor) over monthly or longer time scales can be neglected (Trenberth 1999 and references therein). More recently, the second assumption was dropped in Dominguez et al. (2006) by developing a dynamic precipitation recycling model. Their new model predicts recycling ratios that are 12%–33% larger at a monthly level than previous methods that neglect the change in moisture storage in the atmosphere. These bulk diagnostic approaches for precipitation recycling consider the land surface contribution of moisture supply to precipitation, and the computation of the recycling ratio is relatively easy. However, these approaches do not consider how land surface properties alter atmospheric processes (e.g., stability, circulation), which also affect precipitation. In other words, the recycling ratio does not predict the dynamic changes in rainfall following changes in $E$ or atmospheric moisture fluxes (Eltahir and Bras 1996).

Complementary to the recycling ratio approach, water vapor tracers have also been used in numerical models to calculate the local versus remote geographic (land or ocean) sources of precipitation over a region (Druyan and Koster 1989; Numaguti 1999). For instance, Bosilovich and Schubert (2002) provided the percent contribution of surface $E$ from various (local, adjacent, or remote) regions to the total precipitation in a given region over North America (NA). This approach has been used to compute the precipitation recycling ratio that is quite different from the values using the earlier-mentioned bulk diagnostic approach (Bosilovich and Schubert 2002). The major limitation on the accuracy of the recycling estimates is the veracity of the numerically simulated hydrological cycle.

Because soil moisture $S$ provides the memory for the surface–precipitation coupling, extensive research has also been done on soil moisture time scales. As an example, Wang et al. (2006) demonstrated the different time scales of different water reservoirs of the vegetation–soil system with the shortest and longest time scales for canopy-intercepted water and vegetation rooting zone water, respectively. Furthermore, while soil water and $E$ have the same time scales in a one-layer bucket model, they have quite different time scales when canopy, surface soil layer, and vegetation rooting zone are modeled separately. While the interpretation of results from this approach is straightforward, the linkage to the $E$–$P$ coupling is difficult to quantify.

To directly address the land–precipitation coupling, regional and global models have been used in numerous studies. In particular, 12 global modeling groups participated in the Global Land–Atmosphere Coupling Experiment (GLACE), which focuses on the quantification of the degree to which anomalies in land surface (e.g., soil moisture) can affect summertime rainfall generation (Koster et al. 2006; Guo et al. 2006). GLACE requires two 16-member ensemble simulations: in one ensemble, the 16 simulations differ in their initial conditions, and the soil moisture values at every time step from one member (denoted as W1) are saved in a data file; the other ensemble is the same as the first one, except that the model-predicted soil moisture values in the rooting zone and below are replaced at every time step with values from W1. Then an $\Omega$ index is defined to measure the similarity among 16 members of an ensemble, and the difference between the two ensembles (i.e., $\Delta\Omega$) is used to quantify the strength of soil moisture–precipitation coupling. Similarities in the spatial patterns of $\Delta\Omega$ among 12 models are then used to pinpoint multimodel ''hot spots'' of land–precipitation coupling, including large regions of Africa, central North America, and India (Koster et al. 2006). Large geographic variations of $\Delta\Omega$ with a given model and the large model-to-model differences are also found, and they are primarily caused by the $S$–$E$ formulations, even though the intermodel differences in the $E$ versus $P$ connection also play a key role (Guo et al. 2006). Besides the

TABLE 1. Summary of datasets used. No direct evaporation measurements were used in any of the datasets.

| Name | Type | Period | Resolution | Note | Reference |
|---|---|---|---|---|---|
| NCEP–NCAR | Global reanalysis | 1958–2006 | 2.5° | No *P* assimilation | Kalnay et al. (1996) |
| ERA-40 | Global reanalysis | 1957–2002 | 2.5° | No *P* assimilation | Uppala et al. (2005) |
| NARR | NA reanalysis | 1979–2002 | 30 km | *P* assimilation | Mesinger et al. (2006) |
| VIC | NA offline land | 1950–2000 | 1/8° | Observed *P* | Maurer et al. (2002) |
| CCSM3 | Global model | 50 yr | 2.8° | Simulated *P* | Collins et al. (2006) |
| CCSM3 ($2 \times CO_2$) | Global model | 50 yr | 2.8° | Simulated *P* | Collins et al. (2006) |
| RAMS | NA model | 1950–2002 | 35 km | Simulated *P* | Castro et al. (2007) |

$\Delta\Omega$ index, Wang et al. (2007) proposed an alternative ($\Delta\Phi$) index to quantify the soil moisture–precipitation coupling, and they demonstrated that these two indexes represent different aspects of precipitation predictability in ensemble prediction, with the former ($\Delta\Omega$) emphasizing the predictability of temporal variability and the latter ($\Delta\Phi$) emphasizing the predictability of the mean.

In contrast to the earlier-mentioned modeling studies in which the soil moisture data from a single simulation are used for all simulations in an ensemble, model precipitation values for land models are replaced by the same hybrid observation–reanalysis precipitation data in all simulations in an ensemble (Dirmeyer 2006). On the basis of the analysis of the results from this and the control ensembles, Dirmeyer (2006) found that, globally, fewer than 10% of the signal of any change in precipitation survives the complete circuit of the hydrological cycle (from precipitation to soil moisture, from soil moisture to evapotranspiration, and from evapotranspiration to precipitation) for a particular model, even though there is a great deal of variability regionally.

The advantages of these modeling studies are that the land–precipitation coupling strength can be quantified, and the multimodel averaging procedure in GLACE removes peculiar results from individual models. However, the GLACE approach is still subject to deficiencies shared by multiple models and requires substantial computational resources. More importantly, all these modeling studies are unable to address the realism of the simulated coupling strength, primarily because direct measurements of land–atmosphere interaction at large scales do not exist.

Attempts have also been made to synthesize different approaches to quantify land–atmosphere interactions. For instance, Dirmeyer et al. (2009) combined the characteristics of persistence of soil moisture anomalies, strong soil moisture regulation of evaporation rates, and reinforcement of water cycle anomalies through recycling to present a composite assessment of global land–atmosphere feedback strength as a function of season.

Despite these progresses, our understanding of the land–precipitation coupling remains limited, and large discrepancies still exist from different studies (e.g., Koster et al. 2006; Seneviratne et al. 2006; Wang et al. 2007; Notaro 2008; Zhang et al. 2008). In fact, it is claimed in Koster et al. that, even if perfect measurements of precipitation and *E* in a region were attainable, isolating the effect of *E* on rainfall in the presence of the more dominant effect of rainfall on *E* would prove to be problematic.

Recognizing the importance of the land–precipitation coupling strength and the difficulty in addressing it, the question becomes, is it possible to develop a new index that is easy to compute based on existing observational data and reanalyses as well as standard climate model output for the estimation of the land–precipitation coupling strength? This paper represents our multiyear attempt in this direction. It does not solve this difficult problem; instead, it attempts to provide a simple index that is easy to compute and straightforward to interpret and hence contributes to the better understanding of this issue. Section 2 discusses the data and presents our new index. Results based on various datasets and regional and global model outputs are discussed in section 3, while conclusions are given in section 4.

## 2. Data and method

### *a. Data and model output*

Because of its large spatial and temporal variability (including intermittency), precipitation is one of the most difficult atmospheric variables to measure. While it can be directly measured by using rain gauges, gauge data are not available over unpopulated land regions and most oceanic regions, and the conversion of point values on a sparse irregular grid into areal means introduces sampling errors. Precipitation can also be measured by radars and satellite remote sensing (e.g., Zeng 1999). Compared with precipitation, *E* is even more difficult to measure, and accurate *E* measurements are simply not available globally or even regionally. Recognizing these difficulties, our strategy here is to use data from different sources (as summarized in Table 1) to see if we can reach any conclusions that are relatively robust.

First, we will use the global 2.5° monthly *P* and *E* data from the 40-yr European Centre for Medium-Range

Weather Forecasts (ECMWF) Re-Analysis from the period 1957–2002 (Uppala et al. 2005) and the National Centers for Environmental Prediction–National Center for Atmospheric Research (NCEP–NCAR) reanalysis from the period 1958–2006 (Kalnay et al. 1996). Both variables are model derived, but they are constrained by observational data (without using observed precipitation). Significant biases have been found in the hydrological cycle of both reanalyses (e.g., Trenberth and Guillemot 1998; Hagemann et al. 2005; Lucarini et al. 2007) because of model deficiencies and the failure to directly assimilate observational precipitation. Furthermore, the data assimilation process does not conserve water vapor; thus, the atmospheric moisture budget is not balanced (e.g., Roads et al. 2003).

We will also use the 30-km monthly $P$ and $E$ data from the North American Regional Reanalysis (NARR) from the period 1979–2002 (Mesinger et al. 2006). Compared with the earlier-mentioned global reanalyses, NARR directly assimilates observed hourly $P$ and has a much higher spatial resolution and better accuracy.

In addition to these reanalyses' data using land–atmosphere coupled modeling systems, we will use the North American 1/8° monthly $P$ and $E$ data from the period 1950–2000 (Maurer et al. 2002). The precipitation data were primarily based on surface rain gauge data, while the evaporation values were computed using the Variable Infiltration Capacity (VIC) land model forced by observed precipitation and near-surface air temperature and other derived near-surface atmospheric data. VIC is a macroscale terrestrial hydrologic model that balances both surface energy and water over each model grid.

Furthermore, we will evaluate the monthly $P$ and $E$ from the NCAR Community Climate System Model, version 3 (CCSM3). CCSM3 is a fully coupled global climate model that simulates the earth's past, present, and future climate states (Collins et al. 2006). Model output for 50 yr from the control run and the $2 \times CO_2$ run at T42 (i.e., 2.8°) horizontal resolution will be used.

Besides global model output, we will also evaluate North American monthly $P$ and $E$ for summer from the Regional Atmospheric Modeling System (RAMS; Castro et al. 2007). Boundary conditions for these simulations were provided by the NCEP–NCAR reanalysis for the period 1950–2002. The main intent in Castro et al. (2007) was to demonstrate the improved performance of RAMS (as a regional climate model) over a global model or global reanalysis in the representation of North American warm-season climate. The RAMS output is of interest to analyze because of the increase in coupling strength during the warm season (to be discussed later) and the relatively high spatial resolution (35 km), as compared to a global model such as CCSM3.

The CCSM3 simulations are roughly equivalent to the two reanalyses in grid spacing and physical parameterizations, so the only real difference is that data from various sources were assimilated in the reanalyses, while energy, water, and mass are conserved in the global model. Similarly, the RAMS simulations are roughly equivalent to NARR in grid spacing and physical parameterizations, so the only real difference is that various data (particularly precipitation) were assimilated in NARR, while the other is a pure regional climate model with just lateral boundary forcing and some weak internal nudging.

### b. Method

For each area (or model grid box), the vertically integrated water vapor balance equation in the atmosphere is

$$P = E + C \quad \text{and} \quad C = F_{\text{in}} - F_{\text{out}} - \partial W/\partial t + \alpha, \tag{1}$$

where $W$ is the vertically integrated water vapor (i.e., precipitable water) and $\partial W/\partial t$ can be neglected at monthly or longer time scales, $\alpha$ is an artificial residual term, and $F_{\text{in}}$ and $F_{\text{out}}$ are the inflow and outflow of atmospheric moisture over all the boundaries of the area divided by the area, respectively, so that $(F_{\text{in}} - F_{\text{out}})$ represents the convergence of moisture flux. For atmospheric models, $\alpha$ is zero because of the explicit consideration of water vapor conservation. For data assimilation, $\alpha$ is not zero. In fact, it is relatively large in global reanalysis (e.g., Dominguez et al. 2006), but it is much smaller in the regional reanalysis (Mesinger et al. 2006). For offline land data (e.g., Maurer et al. 2002), atmospheric processes are not considered, and $\alpha$ is not relevant.

As mentioned in section 1, it was thought in the early twentieth century that the ratio of $E/P$ represents the land contribution to precipitation. This is incorrect because $E$ needs to compare with $F_{\text{in}}$ rather than $(F_{\text{in}} - F_{\text{out}})$. Furthermore, part of $E$ is advected out of the area, contributing to $F_{\text{out}}$. Previous bulk diagnostic approaches on precipitation recycling addressed the relative importance of $E$ versus $F_{\text{in}}$ (e.g., Dominguez et al. 2006); however, they did not address the relation of the variation of $P$ versus that of $E$ (e.g., Eltahir and Bras 1996), which is the purpose of our work.

Since (1) is valid for one month, it is also correct for that month averaged over all the years with data, so that it is also valid for the deviation from the climatological monthly mean:

$$P' = E' + C', \tag{2}$$

where each variable is a function of month and year. In our initial attempt (K. Fling et al. 2003, unpublished manuscript), it was argued that, if there is an $E - P$ coupling, it

is necessary that $P'$ correlates with $E'$. Furthermore, this correlation $r_{P,E}$ needs to be compared with that between $P'$ and $C'$ [computed as $(P' - E')$], denoted as $r_{P,C}$. This correlation ratio $\kappa = r_{P,E}/r_{P,C}$ was then used to estimate the $E - P$ coupling strength. While the qualitative results from this parameter are still correct (e.g., the land surface effect on local precipitation is more important in summer than in winter and it is, in general, not as important as the atmospheric moisture convergence), the quantitative interpretation of $\kappa$ turned out to be difficult (to be discussed further later).

As an improvement over our earlier effort, we can rewrite (2) as

$$\sum_{i=1}^{N} P_i'^2 = \sum_{i=1}^{N} P_i' E_i' + \sum_{i=1}^{N} P_i' C_i', \tag{3}$$

where the subscript $i$ denotes month and $N$ denotes the years of data. Then, we define our new indicator of the land–precipitation coupling strength as

$$\Gamma = \sum_{i=1}^{N} P_i' E_i' \Big/ \sum_{i=1}^{N} P_i'^2. \tag{4}$$

The time series of $P_i'$ and $E_i'$ as well as the $\Gamma$ values over two grid cells using various datasets and model outputs will be presented later (Figs. 10 and 11).

Our earlier parameter $\kappa$ can be related to our new parameter $\Gamma$ as

$$\kappa = \frac{\Gamma}{1 - \Gamma} \frac{\sigma_C}{\sigma_E}, \tag{5}$$

where $\sigma_C$ and $\sigma_E$ are the standard deviations of $C'$ and $E'$, respectively. Assuming $\sigma_C$ is comparable to $\sigma_E$, $\kappa$ would be much larger than $\Gamma$ if $\Gamma$ is (usually) between 0 and 1; $\Gamma$ can also be related to $r_{P,E}$ as

$$\Gamma = r_{P,E} \frac{\sigma_E}{\sigma_P}. \tag{6}$$

No specific assumptions are made in the derivation of (4), and monthly $P$ and $E$ are standard model output. Our new parameter $\Gamma$ is easy to compute, and it represents the fractional contribution of the covariance between monthly precipitation deviations (from its climatological mean) and monthly evapotranspiration deviations to the variance of precipitation deviations. Note that the derivation of (3) is not new, and equations similar to (3) have been widely used for different purposes. For instance, similar equations were used to quantify the dominant balances and exchanges of the atmospheric water cycle at diurnal, annual, and intraseasonal time scales using reanalysis data for 3 yr (Ruane and Roads 2008). What is new here is to compute $\Gamma$ in (4) using multidecadal monthly data or model output to characterize the land–precipitation coupling.

If the land–precipitation coupling is weak, then $\Gamma$ should be close to zero. In other words, a relatively large $\Gamma$ is a necessary condition for a relatively strong land–precipitation coupling. Furthermore, a higher $\Gamma$ is most likely to indicate a stronger coupling over most areas, even though special situations may be constructed in which a higher $\Gamma$ does not necessarily correspond to a stronger coupling. The complexity over special situations may be caused by the fact that $E'$ and $C'$ are not entirely independent. For instance, water vapor from evaporation could be carried out of the grid cell by wind. The $\Gamma$ values do not provide causality either.

For reanalyses, climatological mean errors in $P$ or $E$ do not affect the computation of $\Gamma$, because only deviations (from climatological means) are used in (4). While the moisture convergence in the atmosphere ($F_{\text{in}} - F_{\text{out}}$) in (1) is generally regarded as more reliable than $E$, it is generally not archived and has to be computed from usually 6-hourly reanalysis data. The reanalysis data have also been interpolated from model (sigma) levels to pressure levels, destroying much of the detail in the lower atmosphere that contributes to the final integrated values of $F_{\text{in}}$ and $F_{\text{out}}$. Furthermore, because of the existence of residual term $\alpha$ in (1) and the uncertainties in $P$, it will be our future task to directly use the deviations of ($F_{\text{in}} - F_{\text{out}}$) to compute the $E$ deviations.

Note that, instead of the covariance in (4), time-delayed covariance of $\sum_{i=1}^{N} P_i' E_{i-1}'$ (with the subscript $i$ denoting month) can also be computed. However, even this lagged covariance may not represent the causality because of the complicated interaction of $P'$, $E'$, and $C'$. Furthermore, the ratio of such lagged covariance over the variance of $P'$ does not represent the fractional contribution anymore. For these reasons, only $\Gamma$ values in (4) are computed in this study.

Compared with previous studies, $\Gamma$ is most similar to the parameter $\lambda$ in Notaro (2008), which is computed as the ratio of the lagged covariance between $P$ and total column $S$ over the lagged covariance of $S$. Both $\Gamma$ and $\lambda$ are easy to compute, without doing additional modeling experiments. Here, $\Gamma$ has a clear physical meaning without making any assumptions, but it does not provide causality. The interpretation of $\lambda$ as the $S - P$ feedback parameter depends on two assumptions: (i) the lagged covariance between the precipitation perturbations (generated internally by atmospheric processes) and $S$ can be neglected and (ii) the atmospheric response time is much shorter than the monthly time scale. These assumptions may not be valid in some situations. For instance, internal atmospheric dynamics may generate 30–60-day oscillations in the tropics

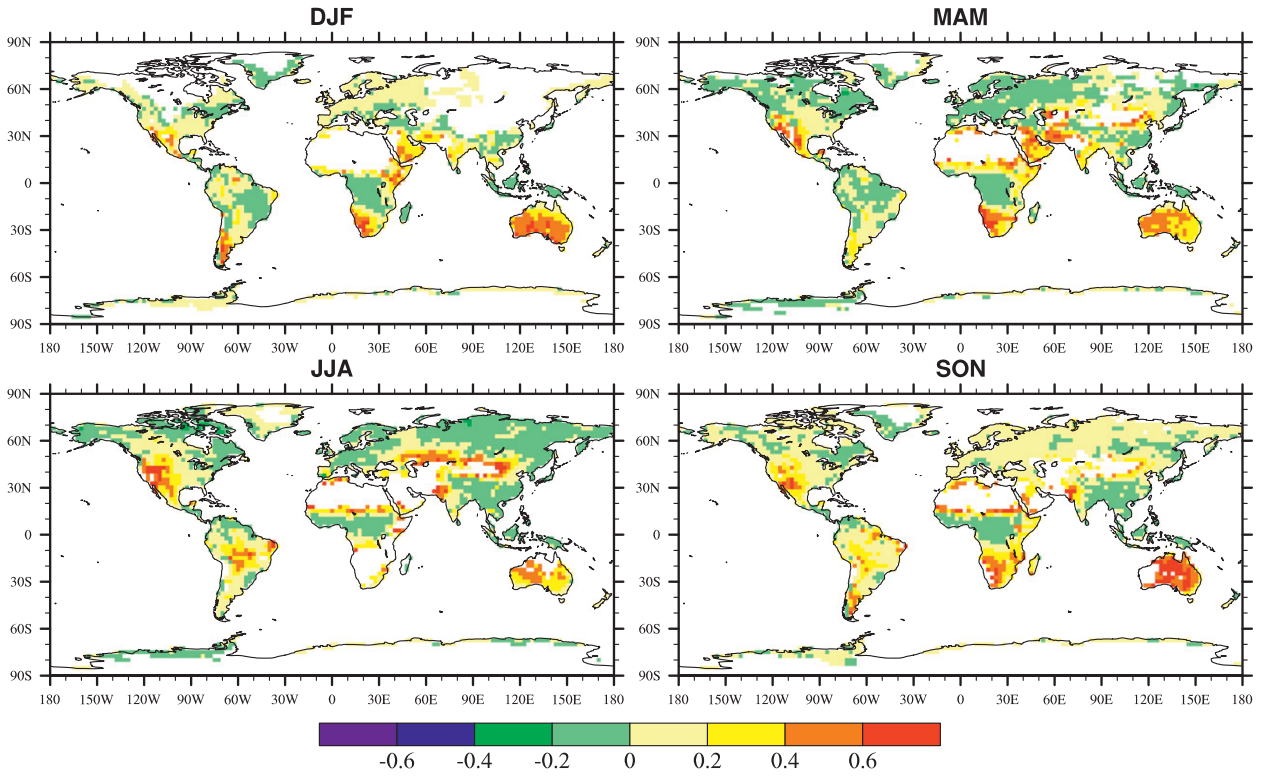


FIG. 1. Seasonal Γ distributions based on the ECMWF reanalysis data. Results over oceans and those over land with the standard deviation of seasonal $P$ less than 0.2 mm day$^{-1}$ are shaded.

(Zhang 2005). Here, $\lambda$ is more closely related to causality than Γ, but it still does not represent the causality directly, as cautioned in Salvucci et al. (2002) and Wei et al. (2008).

## 3. Results

### a. *Results based on global and regional reanalysis data*

Figure 1 shows the seasonal Γ distribution using the ECMWF reanalysis data. The statistical significance of the results can be estimated as the same as that of the $r_{P,E}$ based on (6). It is found that Γ values more than 0.2 in magnitude are significant at the 5% level in Fig. 1. Similar to Koster et al. (2006), areas with relatively high Γ values (e.g., $\Gamma > 0.4$) are defined as hot spots here. It is clear from Fig. 1 that the hot spots move with season. Over the Northern Hemisphere, the hot spots in boreal summer [June–August (JJA)] include the western and central parts of North America, part of the Eurasia midlatitude, and Sahel. For transition seasons [September–November (SON) and March–May (MAM)], these hot spots still exist to a certain degree but with smaller Γ values. They largely disappear in boreal winter [December–February (DJF)]. Over the Southern Hemisphere, the hot spots in austral summer (DJF) include most of Australia, Argentina, and South Africa. For transition seasons (SON and MAM), these hot spots (except Argentina) still exist. In austral winter (JJA), the hot spot disappears over South Africa and is significantly weakened over Australia, while a new hot spot appears over the central plains of South America.

The summertime land–precipitation coupling strengths have been discussed based on GLACE (Koster et al. 2006) and on the lagged soil moisture–precipitation covariance analysis of results from 19 Intergovernmental Panel on Climate Change (IPCC) models (Notaro 2008). The existence of hot spots over North and South America, Eurasia, and North Africa in the summer (JJA) panel of Fig. 1 is qualitatively similar to those in Koster et al. (2006, their Fig. 10) and Notaro (2008, his Fig. 3), even though exact geographic locations differ. All three agree with each other on the hot spot over northern India. The hot spot over the equatorial Africa (with rain forest) and Sahel (with grasses, shrubs, and savannas) is the largest in Koster et al. and Notaro, while it is smaller in geographic area and appears primarily at the semiarid transition zone between the Sahara Desert and the tropical forest in the JJA panel of Fig. 1. In North America, the hot spot that

exists over the central part in Koster et al. covers both the western and central parts in the JJA panel of Fig. 1, and covers both the central and eastern parts in Notaro. In Eurasia, there are no hot spots in Koster et al., while results in the JJA panel of Fig. 1 agree with those in Notaro (i.e., with a hot spot along a midlatitude band). In South America, the hot spot occurs over the central Amazon in Koster et al. and in the northern Amazon in Notaro, while it occurs over the central plains (rather than the tropical forest) in the JJA panel of Fig. 1. Both the JJA panel of Fig. 1 and Notaro show a hot spot over Australia, while there is none in Koster et al. While Notaro shows a hot spot over Indonesia, there is none in the JJA panel of Fig. 1 or Koster et al.

Dirmeyer et al. (2009) presented a composite assessment of global land–atmosphere feedback strength as a function of season. Over North America, both Fig. 1 here and Fig. 6 in Dirmeyer et al. show the strong land–precipitation coupling strength over western and central parts for some seasons. However, the overall coupling is strongest in summer in Fig. 1, but it is in spring in Dirmeyer et al. Furthermore, there is a hot spot over central North America in winter (DJF) in Dirmeyer et al., while there is none in Fig. 1. Both show a hot spot over Eurasia but, again, the seasonality is different with the maximum coupling occurring in spring in Dirmeyer et al. and in summer in Fig. 1. The hot spot over Sahel occurs in summer and fall in Fig. 1, while it occurs in fall only in Dirmeyer et al. Both show the hot spot over Australia, but Fig. 1 shows the minimum coupling in austral winter (JJA), while it occurs in austral summer (DJF) in Dirmeyer et al. Both show strong coupling in South Africa in MAM and weak coupling in JJA; however, the coupling for other two seasons is also strong in Fig. 1 but weak in Dirmeyer et al. Both show the JJA hot spot over the central plains of South America; however, the coupling is strongest in Argentina in austral summer in Fig. 1 but strongest in two areas of South America in austral autumn (MAM).

To better understand the $\Gamma$ values, Fig. 2 compares the geographic distribution of $\Gamma$, $\kappa$, and $r_{P,E}$, which are quantitatively linked through (5) and (6). Here, $r_{P,E}$ is dominated by the effect of $P$ on $E$ (through soil moisture), and the areas covered by $r_{P,E}$ values higher than 0.4 (i.e., statistically significant at the 1% level) in Fig. 2a are much greater than those indicated by the $\Gamma$ values in Fig. 2d. The GLACE multimodel analysis in Guo et al. (2006) shows that the existence of hot spots of land–atmosphere coupling in the transition zones between dry and wet areas is because of the coexistence there of a high sensitivity of $E$ to soil moisture and a high temporal variability of the $E$ signal. In particular, Guo et al. (2006) concluded that an evaporation rate that varies strongly and consistently with soil moisture tends to lead to a higher $S$–$P$ coupling strength. Since $\Gamma$ represents the product of $r_{P,E}$ and $\sigma_E$ normalized by $\sigma_P$ in (6), it explicitly represents the effect of $P$ on $E$ (through soil moisture) and may implicitly reflect part of the feedback from $E$ to $P$ (through $\sigma_E$ which is correlated with the coupling strength mentioned in Guo et al.).

The correlation ratio $\kappa = r_{P,E}/r_{P,C}$ in Fig. 2b provides a useful constraint in the interpretation of $r_{P,E}$ in Fig. 2a: $r_{P,E}$ needs to be statistically significant and also compared with $r_{P,C}$. However, areas with high $\kappa$ values are nearly the same as those with high $r_{P,E}$ values, and quantitative interpretation of $\kappa$ remains difficult. For instance, $\kappa$ is larger than 1.2 over a few areas in Fig. 2b, which seems to (incorrectly) imply that land effect on precipitation is more important than atmospheric advective processes. In contrast, with a clear physical meaning from (4), $\Gamma$ is easy to interpret quantitatively in Fig. 2d.

The standard deviation of $P'(\sigma_P)$ is less than 0.1 mm day$^{-1}$ over deserts and permanent ice caps in polar regions (Fig. 2c), while it is much higher over humid regions. Over regions with small $\sigma_P$, the covariance of $P'$ and $C'$ does not have much practical value, while $\Gamma$ might become arbitrarily large. Therefore, $\Gamma$ is computed only over regions with $\sigma_P$ greater than 0.2 mm day$^{-1}$. Evidently the use of 0.1 or 0.3 mm day$^{-1}$ would affect the results over some grid cells but would not affect any conclusions.

Figure 3 shows the $\Gamma$ distributions using the NCEP reanalysis data. As expected, exact $\Gamma$ values differ between Figs. 1 and 3. However, areas with relatively high $\Gamma$ values are similar to each other over most regions except for the overall higher $\Gamma$ values over Australia in the ECMWF reanalysis and the overall higher $\Gamma$ values in the Sahel in the NCEP reanalysis.

One of the deficiencies of both ECMWF and NCEP reanalyses is that they did not assimilate precipitation data. In contrast, NARR did assimilate the observed hourly precipitation. To be comparable with the global reanalysis data, the 32-km NARR $E$ and $P$ data were averaged into 2.5°, which were then used to compute $\Gamma$ values. As an example, the results for July are shown in Fig. 4a. Consistent with both ECMWF and NCEP data, $\Gamma$ values are relatively high over the western and central parts of North America only.

For the computation of the precipitation recycling ratio, the results are very sensitive to the horizontal scales used (e.g., Eltahir and Bras 1996; Trenberth 1999). To address this issue, $\Gamma$ values were also computed at the 32-km resolution and then averaged to 2.5° grid cells, as shown in Fig. 4b. The results in Figs. 4a and 4b are nearly the same, with the differences $<0.1$ in magnitude, indicating that the $\Gamma$ values are insensitive to the horizontal scales.

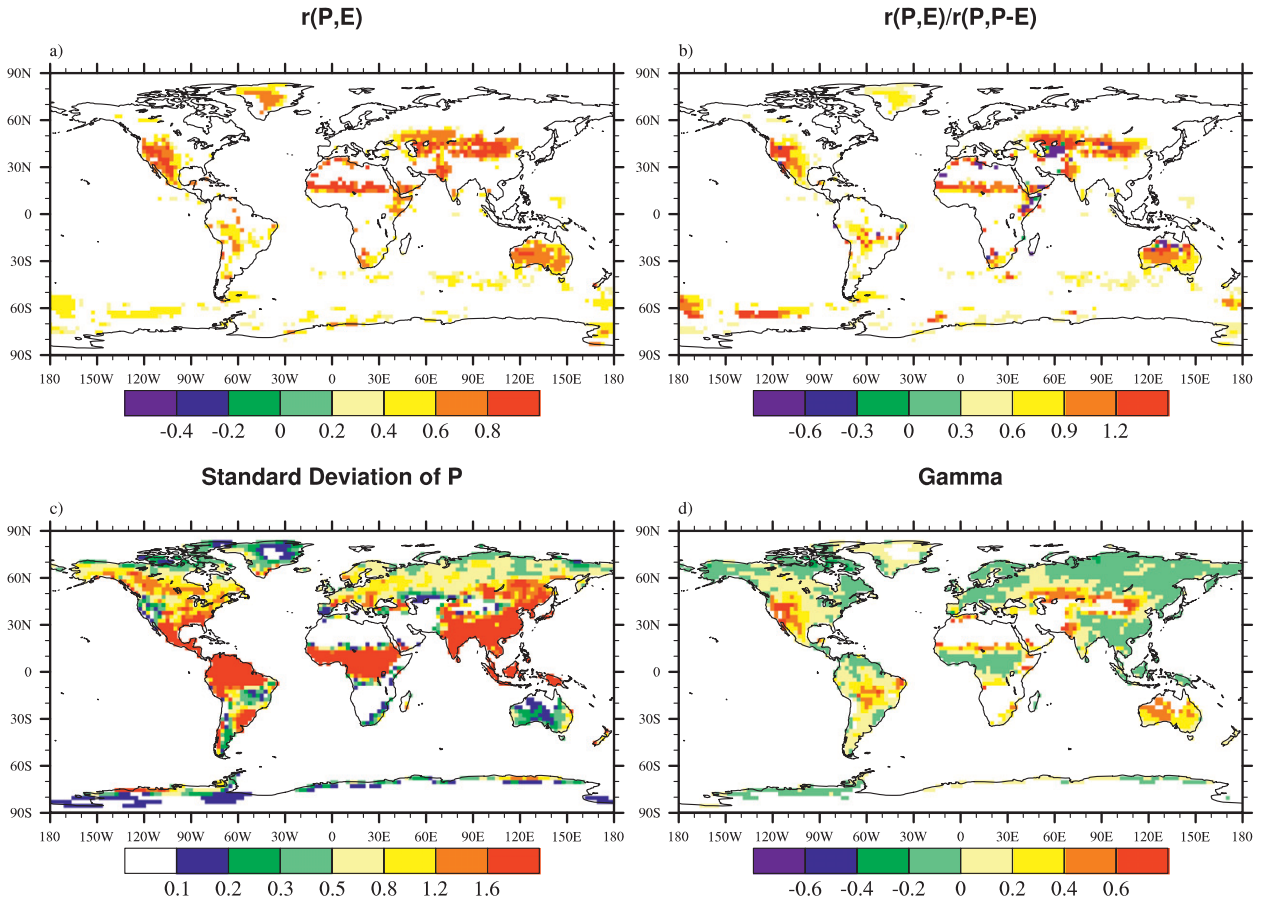


FIG. 2. The summertime (JJA) distributions of (a) $r_{P,E}$, (b) $\kappa$, (c) $\sigma_P$ (mm day$^{-1}$), and (d) $\Gamma$ (same as Fig. 1c) based on the ECMWF reanalysis data.

In the reanalysis data mentioned earlier, the residual term $\alpha$ in (1) is not zero, as also mentioned earlier. The precipitation data from the two global reanalyses also have serious deficiencies. Here, we also use the observed precipitation and the evapotranspiration data derived from the offline VIC land modeling over North America (Maurer et al. 2002). Figure 5 shows that the results are consistent with those from the ECMWF and NCEP reanalyses: higher $\Gamma$ values in summer than in winter, and higher $\Gamma$ values in the western and central parts of Northern America than over the eastern part.

As a synthesis of the results so far, Fig. 6 presents averaged $\Gamma$ distributions for July using all four datasets. Again, the $\Gamma$ values are higher over the western and central parts of North America than over the eastern part. As mentioned before, high $\Gamma$ values may not have practical values if the standard deviation of precipitation $\sigma_p$ is too small. To illustrate this point, three different shadings are used in Fig. 6. The results are shaded in Fig. 6c if $\sigma_p <$ 0.2 mm day$^{-1}$ from all four datasets, which is least restrictive. There are four grid cells with $\Gamma > 0.6$. When only the observed precipitation data as used in VIC are used for shading in Fig. 6a, these grid cells are reduced to one cell only (with $\Gamma > 0.6$). When the criterion is most restrictive (i.e., $\sigma_p < 0.2$ mm day$^{-1}$ from any of the four datasets) in Fig. 6b, there are no grid cells with $\Gamma > 0.6$. To be conservative, the most restrictive Fig. 6b is taken as the synthesis of results in which the hot spot covers the Great Plains (in agreement with Koster et al. 2006) and part of the western United States (in agreement with Zhang et al. 2008).

### b. *Model output analysis*

Because the computation of the $\Gamma$ values is very easy, we have analyzed the regional and global model outputs and results are presented here.

Figure 7 show the results using 50-yr monthly model output from the ocean–atmosphere–land–ice fully coupled CCSM3 (Collins et al. 2006). Compared with data analysis (e.g., Figs. 1 and 3), the model correctly shows higher $\Gamma$ values in the summer hemisphere than in the winter hemisphere. However, the $\Gamma$ values are overall

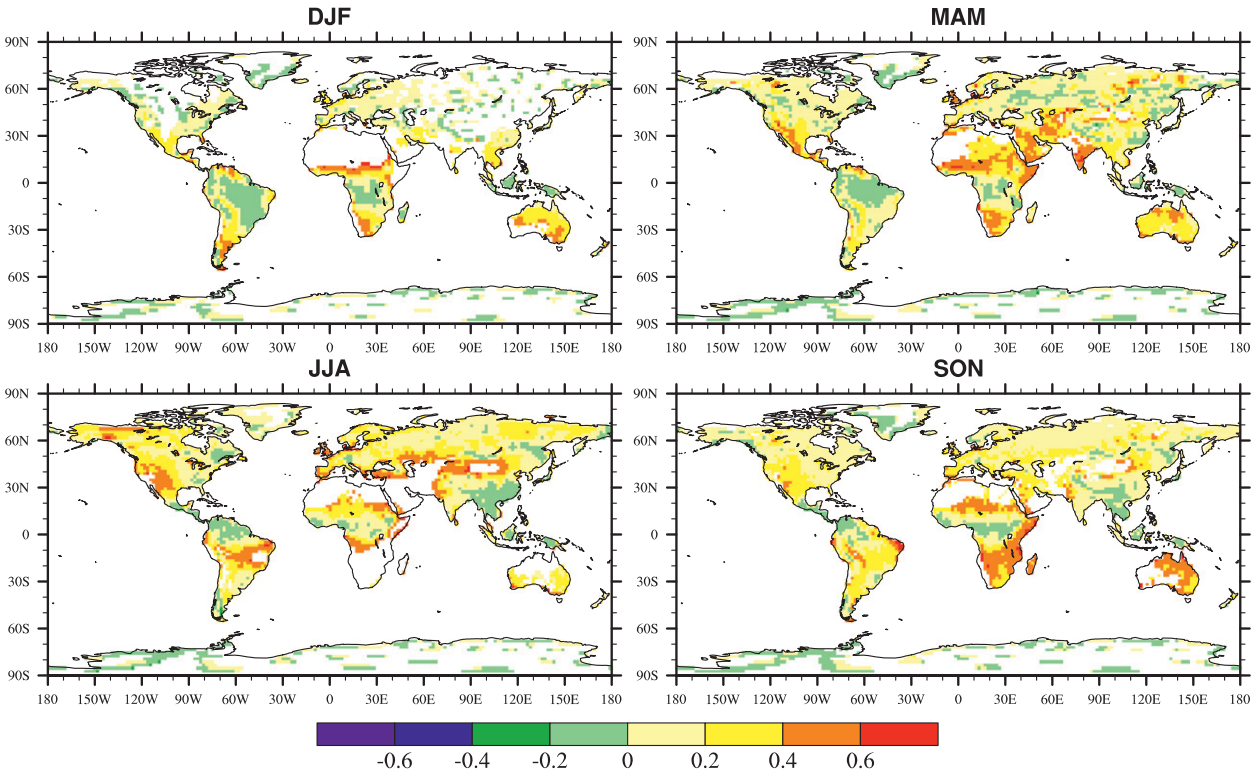


FIG. 3. As in Fig. 1, but using the NCEP reanalysis data.

much higher compared with Figs. 1 and 3. In particular, summertime Γ values over the eastern part of the United States are greater than 0.6, in contrast to the values less than 0.2 in Fig. 6. The strong land–atmosphere coupling in the CCSM3 shown here is consistent with the strong coupling shown by its atmosphere–land coupled components [Community Atmosphere Model, version 3–Community Land Model, version 3 (CAM3–CLM3)] in Koster et al. (2006). This strong coupling is primarily caused by the high sensitivity of atmospheric convection to surface heat flux forcing in CCSM3 (Guo et al. 2006), and to a lesser degree, caused by the severe dry soil bias in CCSM3 (Lawrence et al. 2007).

We have also computed the Γ values using the 50-yr output of CCSM3 with the doubling of $CO_2$, and Fig. 8 shows the differences between the doubling of $CO_2$ and the control CCSM3. There is an increase of Γ values in the warming world over part of the northern high latitudes, eastern North America, and southern Australia in July. Over most of the other regions and for other months, the Γ

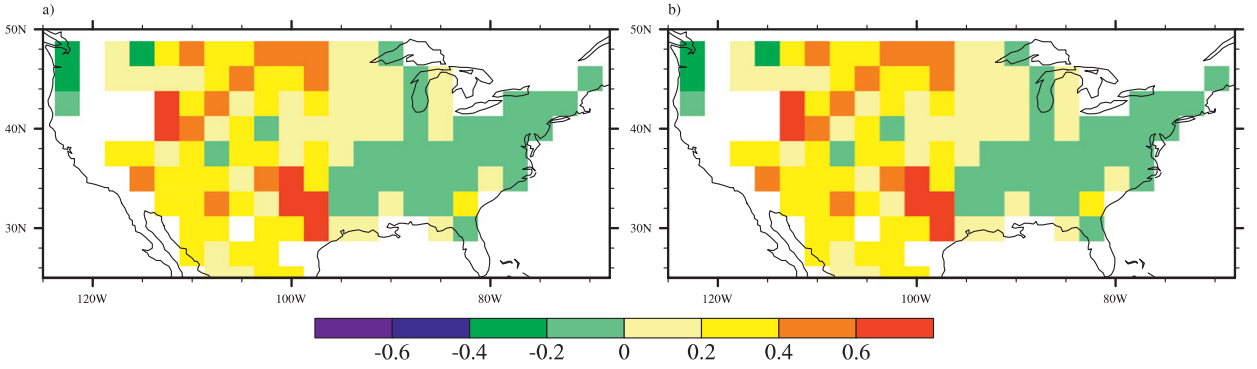


FIG. 4. Monthly Γ distributions in July based on the NARR reanalysis data. The results over oceans and those over land with the standard deviation of monthly $P$ less than 0.2 mm day$^{-1}$ are shaded. (a) The $E$ and $P$ data were averaged from around 32 km to 2.5° and then used to compute Γ. (b) The Γ values at 32-km resolution were computed and then averaged to 2.5°.

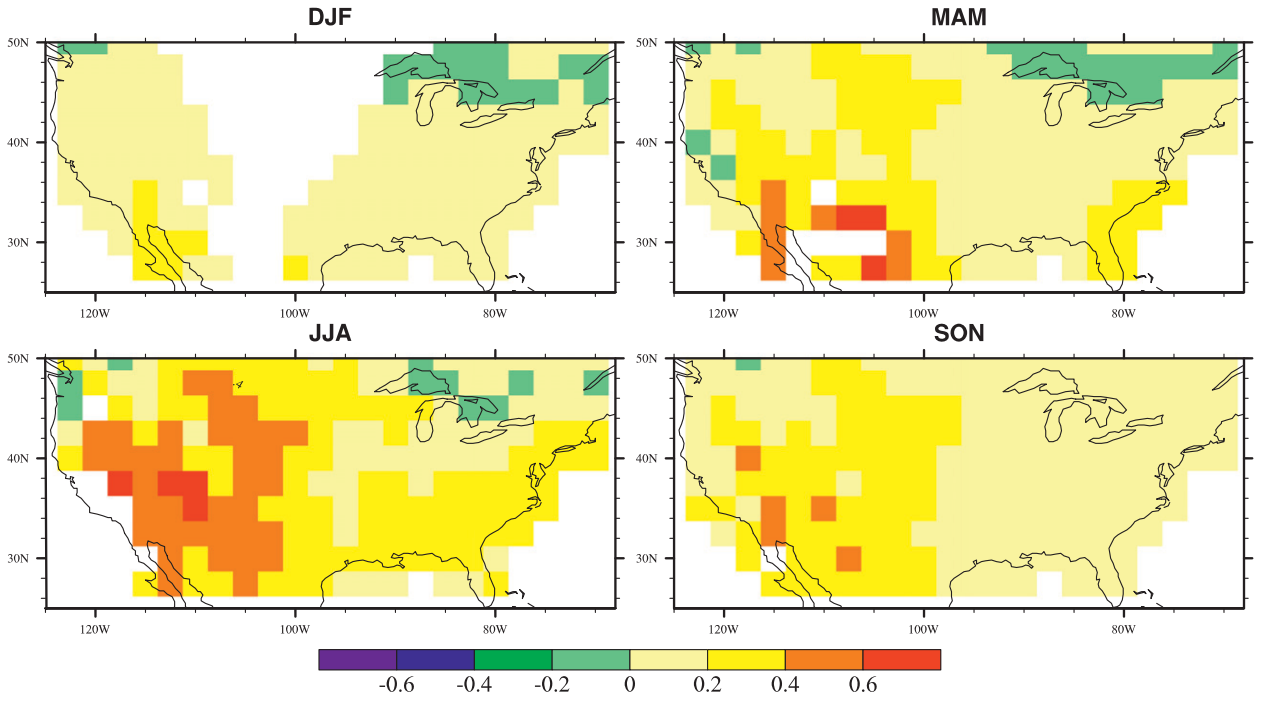


FIG. 5. Seasonal Γ distributions based on the observed $P$ and $E$ data derived from the VIC land model over North America. The results (over land) with the standard deviation of seasonal $P$ less than 0.2 mm day$^{-1}$ are shaded. The $E$ and $P$ data were averaged from 0.125° to 2.5° and then used to compute Γ.

differences are not coherent in space, indicating an overall insensitivity of Γ values to the doubling of $CO_2$.

We have also analyzed the regional climate model output (Castro et al. 2007). Figure 9 shows that the regional climate model (RAMS) is more realistic in producing smaller Γ values over the eastern part of the United States than the global model (CCSM3, Fig. 7), even though these Γ values are still higher than those from data analyses in Fig. 6.

To better understand the results from the analyses of data and model output, Figs. 10 and 11 show the actual monthly $E$ and $P$ anomalies in July over two grid cells over the United States. When the Γ value is relatively high, both $E'$ and $P'$ show significant variations in Fig. 10. Consistent with the overall small Γ differences between the doubling of $CO_2$ versus the control CCSM3 simulations, the difference is just −0.04 over this grid cell. Even though Γ values from CCSM3 and RAMS are generally higher than those using observed and reanalysis data, they are lower at this grid cell.

When the Γ value is low, the variation of $P'$ is still large; however, the variation of $E'$ is small in Fig. 11. For this location, the Γ value (0.04) from RAMS is consistent with the average (0.09) from all four datasets, while the Γ value (0.30) from CCSM3 is much larger than those from data analysis. In contrast to the grid cell in Fig. 10, there is a large Γ difference (0.21) between the doubling of $CO_2$ versus the control CCSM3 simulations.

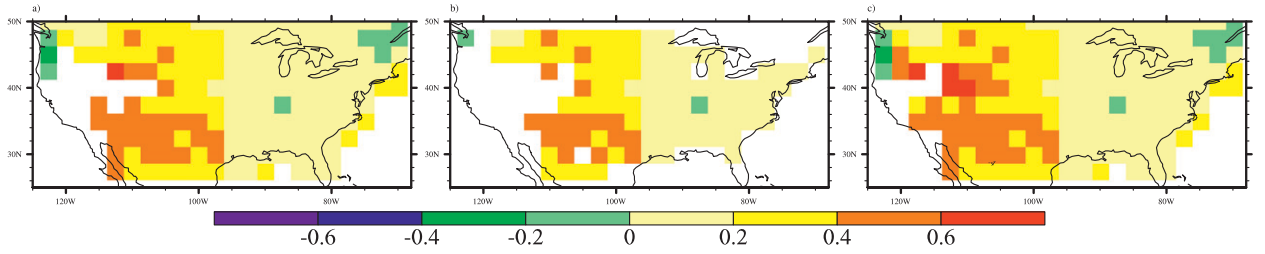


FIG. 6. Average monthly Γ distributions for July over North America using the 2.5° data from global reanalyses (ECMWF, NCEP), regional reanalysis (NARR), and offline land data (VIC). The results (over land) are shaded if the standard deviation of monthly $P$ is less than 0.2 mm day$^{-1}$ using the observed $P$ data as used in (a) VIC, (b) any of the four datasets, and (c) using all four datasets.

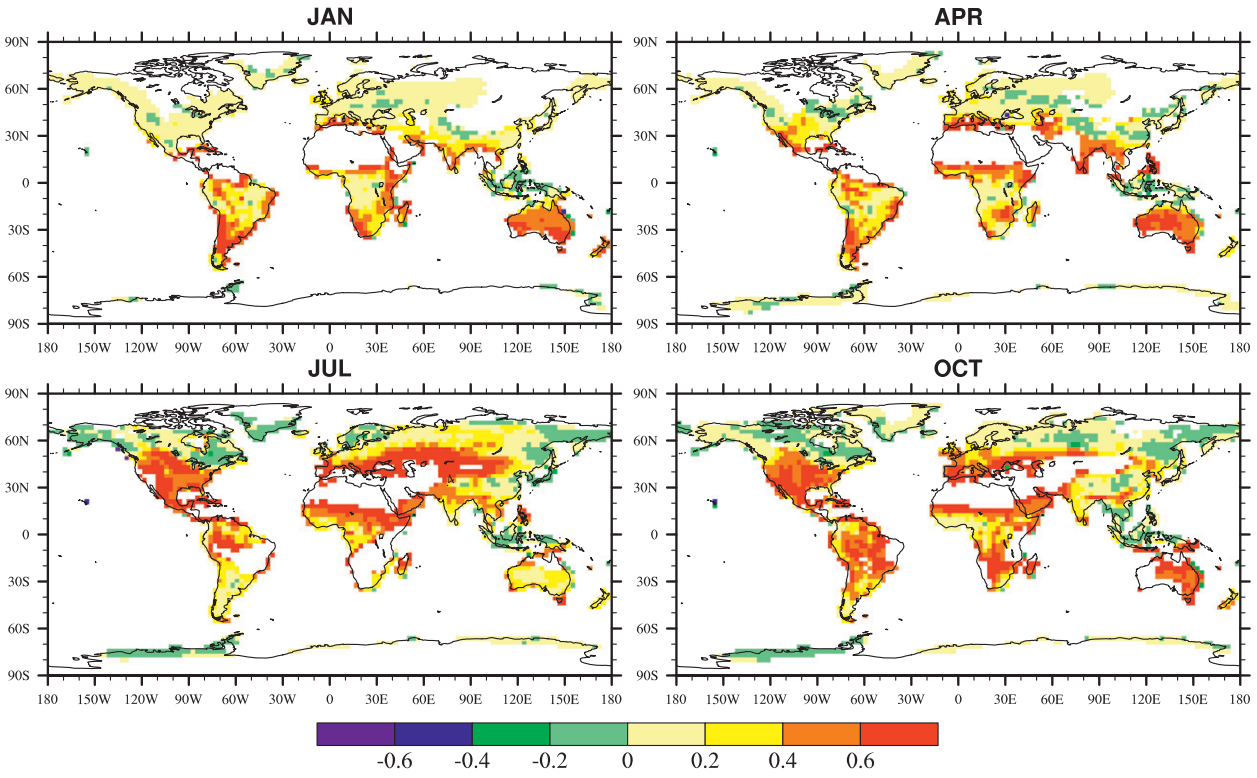


FIG. 7. Monthly averaged Γ in January, April, July, and October based on 50-yr CCSM3 model output. Results over oceans and those over land with the standard deviation of model monthly $P$ less than 0.2 mm day$^{-1}$ are shaded.

## 4. Conclusions

Land–precipitation coupling has been studied for more than a century and has received particular attention in the past 10 years—from water isotope analysis, precipitation recycling ratio analysis, water vapor tracer computation, soil moisture memory evaluation, and direct land–atmosphere coupled modeling. However, our understanding remains limited, and discrepancies still exist from different studies. In this study, a simple parameter—Γ—is proposed to estimate the land–precipitation coupling strength based on the ratio of the covariance between monthly or seasonal precipitation and evaporation anomalies (from their climatological means) over the variance of precipitation anomalies. The Γ value is easy to compute from observations and standard model output and is relatively straightforward to interpret. A relatively high Γ is a necessary condition for a relatively strong land–precipitation coupling.

First, Γ values are computed using the ECMWF and NCEP global reanalyses, and results are similar between them. Results from these global datasets, the NARR regional reanalysis in which precipitation was assimilated, and the observed precipitation along with derived evaporation data indicate that the land–precipitation coupling is stronger in summer and weaker in winter. The strongest coupling (i.e., hot spots) occurs over the western and central parts of North America, part of the Eurasia midlatitude, and Sahel in boreal summer and over most of Australia, Argentina, and South Africa in austral summer.

Then, Γ values are computed using the output from global and regional climate models. The Community Climate System Model, version 3 (CCSM3) shows much higher Γ values, consistent with the strong coupling shown by its atmosphere–land coupled components in Koster et al. (2006). The doubling of $CO_2$ in CCSM3 increases the Γ values over part of northern high latitudes, eastern North America, and southern Australia in July. Over most of the other regions and for other months, the overall spatial pattern of Γ values is not much affected by the doubling of $CO_2$ in CCSM3. The Γ values from the Regional Atmospheric Modeling System (RAMS) are more realistic than those from CCSM3, but they are still higher than those from observations.

The global distribution and seasonal variations of Γ values from the ECMWF and NCEP reanalyses have been compared with previous modeling and data analysis results. While the existence of hot spots in most regions qualitatively agree with each other, the exact geographic locations of these hot spots in summer differ among this

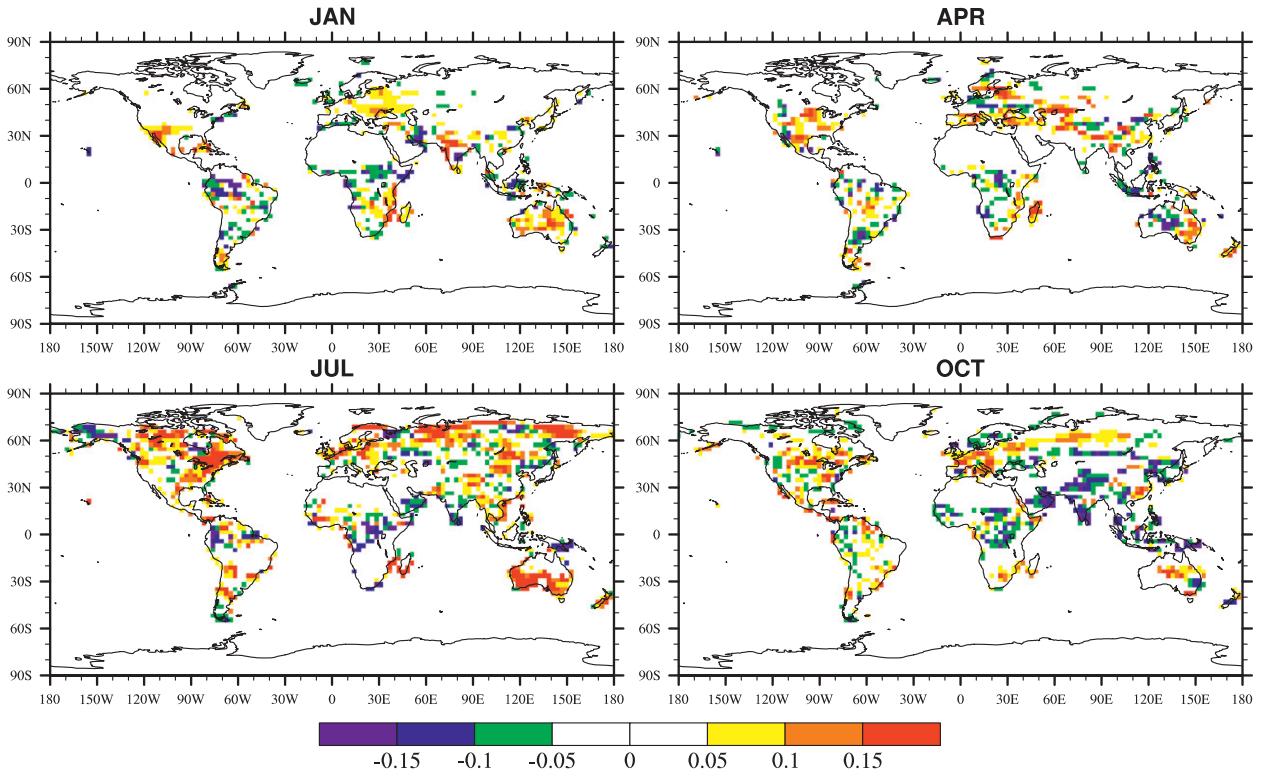


FIG. 8. Difference of monthly averaged Γ in January, April, July, and October based on 50-yr model output from the doubling of $CO_2$ vs control CCSM3 simulations. Results over oceans and those over land with the standard deviation of monthly $P$ from either of the simulations less than 0.2 mm day$^{-1}$ are shaded.

study, the multimodel study of Koster et al. (2006), and the lagged soil moisture–precipitation covariance analysis of IPCC model results in Notaro (2008) or between the latter two studies. While our results show the maximum land–precipitation coupling strength in summer, the maximum coupling occurs in autumn from the data analysis of Dirmeyer et al. (2009).

Our approach can also be compared with previous approaches in general. While the precipitation recycling ratio (e.g., Trenberth 1999) is sensitive to the horizontal

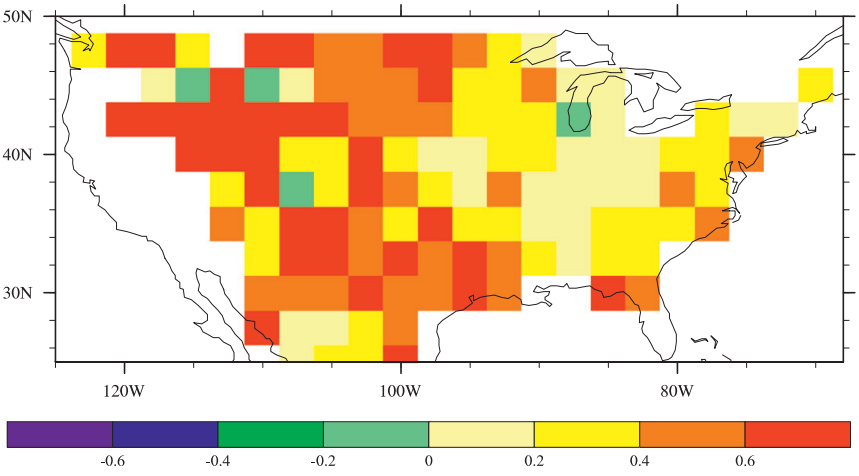


FIG. 9. Monthly averaged Γ in July based on 52-yr RAMS regional climate model output. Results over oceans and those over land with the standard deviation of model monthly $P$ less than 0.2 mm day$^{-1}$ are shaded. The $E$ and $P$ data were averaged from 32 km to 2.5° and then used to compute Γ.

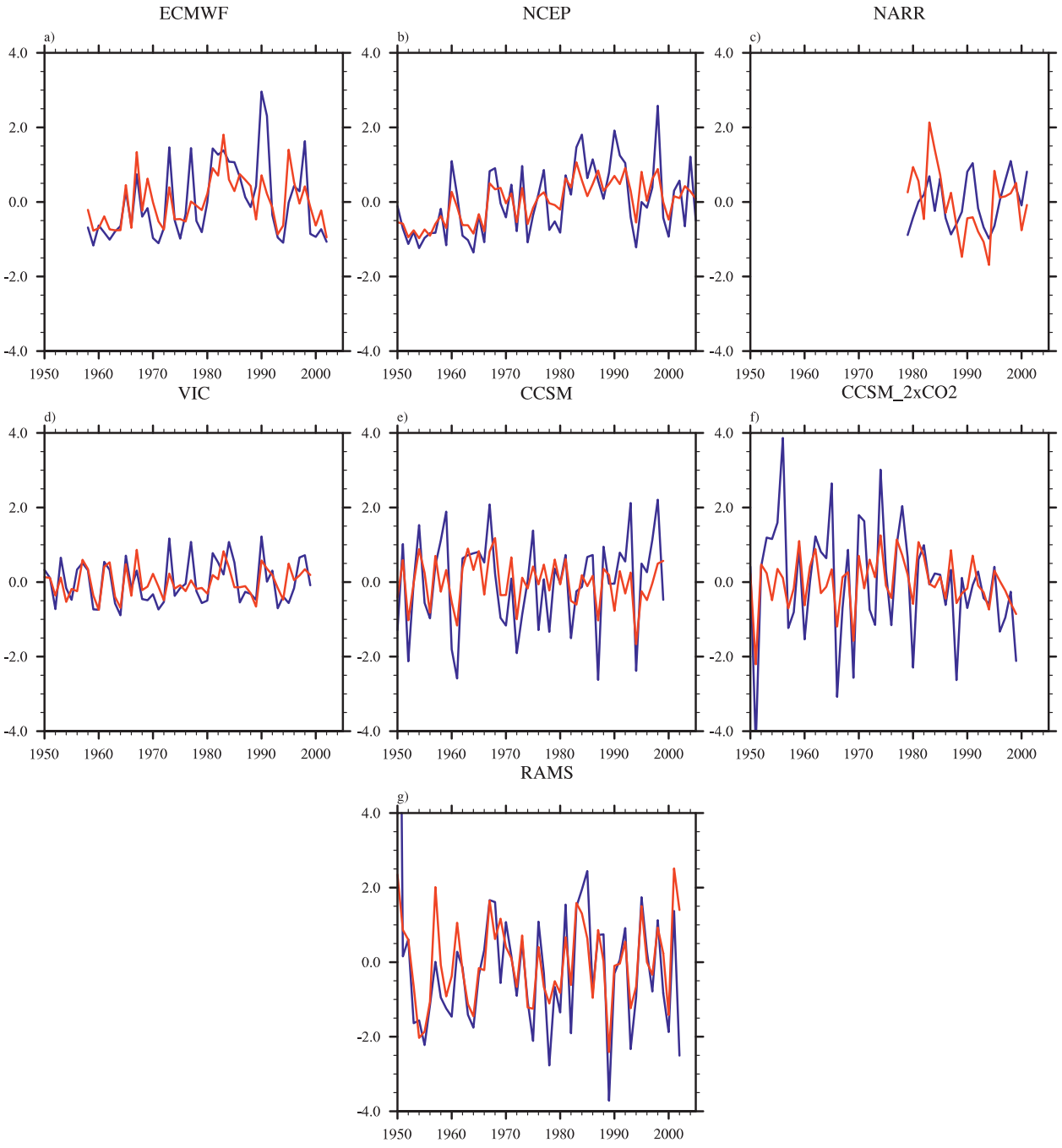


FIG. 10. Time series of July $E$ (red lines) and $P$ (blue lines) anomalies (mm day$^{-1}$) over a grid cell centered at (40°N, 105°W) with relatively large $\Gamma$ values from data analyses: (a) ECMWF (with $\Gamma = 0.45$), (b) NCEP ($\Gamma = 0.50$), (c) NARR ($\Gamma = 0.36$), (d) VIC ($\Gamma = 0.44$), (e) control CCSM3 ($\Gamma = 0.36$), (f) CCSM3 with the doubling of $CO_2$ ($\Gamma = 0.32$), and (g) RAMS ($\Gamma = 0.24$).

scales used, our $\Gamma$ values are not. Both $\Gamma$ values and $\lambda$ values from Notaro (2008) are easy to compute compared with other modeling approaches (e.g., Koster et al. 2006). Here, $\Gamma$ is derived rigorously in (4) and represents the fractional contribution of the covariance between monthly $P'$ and $E'$ to the variance of monthly $P'$, while the interpretation of $\lambda$ as the soil moisture–precipitation feedback parameter depends on two assumptions that may not be valid in some situations. On the other hand, a higher $\Gamma$ is just a necessary—but not sufficient—condition for a strong land–precipitation coupling. For instance, for an idealized situation where $P'$ causes soil moisture

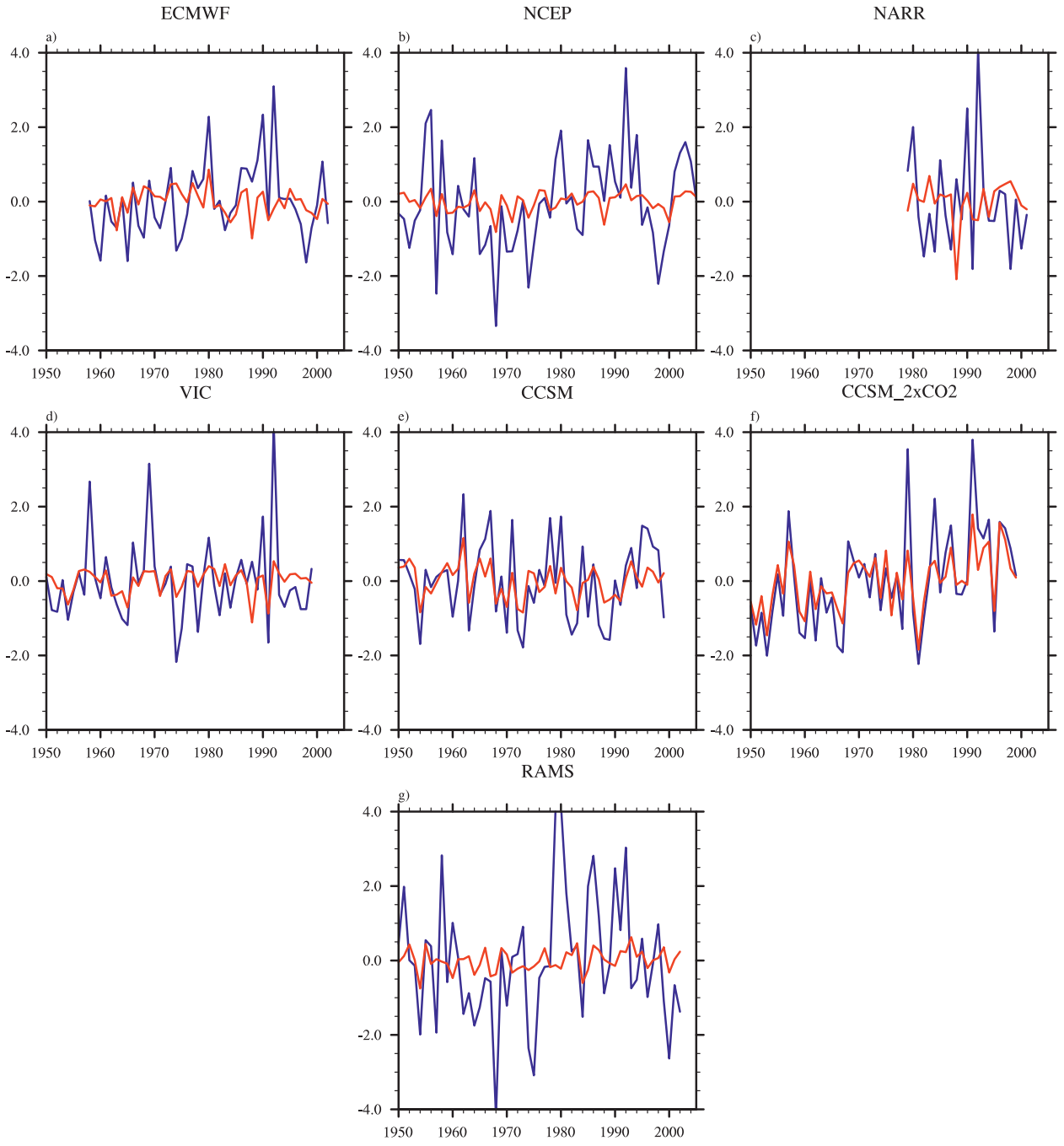


FIG. 11. Time series of July $E$ (red lines) and $P$ (blue lines) anomalies (mm day$^{-1}$) over a grid cell centered at (40°N, 82.5°W) with relatively small $\Gamma$ values from data analyses: (a) ECMWF (with $\Gamma = 0.10$), (b) NCEP ($\Gamma = 0.14$), (c) NARR ($\Gamma = -0.04$), (d) VIC ($\Gamma = 0.16$), (e) control CCSM3 ($\Gamma = 0.30$), (f) CCSM3 with the doubling of $CO_2$ ($\Gamma = 0.52$), and (g) RAMS ($\Gamma = 0.04$).

anomalies and hence $E'$, there would be a high $\Gamma$ value even if there is a minimal feedback from $E'$ to $P'$. Here, $\lambda$ is more closely related to causality than $\Gamma$, but it still does not represent the causality directly. In fact, data analysis, theoretical reasoning, and modeling all indicate that the lagged soil moisture–precipitation correlation could be mainly caused by the combined effect of precipitation variability and the soil moisture memory, so that the lagged correlation does not necessarily imply a causality (Wei et al. 2008). The GLACE modeling approach in Koster et al. (2006) is useful to directly address part of the soil moisture–precipitation coupling problem, but it is computationally expensive and some of its weaknesses have also been identified (e.g., Seneviratne et al. 2006;

Wang et al. 2007; Notaro 2008; Zhang et al. 2008). The composite data analysis in Dirmeyer et al. (2009) considers three factors: soil moisture control of $E$, soil moisture memory, and the precipitation recycling. However, only the correlation of soil moisture and recycling ratio, rather than the recycling ratio itself, was considered. In other words, a high correlation does not necessarily imply a high recycling ratio. Some of its conclusions (e.g., the generally strongest coupling in the transition seasons, rather than during the summer; the weakest coupling in austral summer, rather than in austral winter, over Australia) still need to be further verified.

These comparisons and the earlier-mentioned different results from different approaches both indicate our current lack of understanding of the land–precipitation coupling, and it is difficult to claim which approach is most realistic at present. Our parameter—Γ—is simple to compute and straightforward to interpret and hence provides a good base line for land–precipitation coupling studies. As an example, Γ values can be easily computed from monthly or seasonal output from different global and regional models (e.g., those used in various model intercomparison projects and in the IPCC simulations), and these Γ values could place an individual model's land–atmosphere coupling strength within the broad range of those from various models. As mentioned earlier, CCSM3 shows much higher Γ values, consistent with its strong coupling from GLACE, but the Γ computation is much simpler. Further efforts with creative data analysis and innovative design of model experiments are still needed to better understand the land–precipitation coupling. For instance, the Γ parameter from this study, the $\lambda$ parameter from Notaro (2008), and the composite approach from Dirmeyer et al. (2009) may be combined for the analysis of observational data and model output. Particularly useful for such a study would be the newly available reanalysis data from Modern Era Retrospective-analysis for Research and Applications (MERRA; Bosilovich et al. 2009) with its improved estimates of the hydrological cycle, including the saving of the analysis increments to help address the vexing problem of the lack of closure in (1).

*Acknowledgments.* This work was supported by NOAA (Grant NA07NES4400002) and NASA (Grant NNX09A021G). Francina Dominguez and three anonymous reviewers are thanked for their insightful and helpful comments.

## REFERENCES

Anderson, B. T., G. Salvucci, A. C. Ruane, J. O. Roads, and M. Kanamitsu, 2008: A new metric for estimating the influence of evaporation on seasonal precipitation rates. *J. Hydrometeor.,* **9,** 576–588.

Bisselink, B., and A. J. Dolman, 2008: Precipitation recycling: Moisture sources over Europe using ERA-40 data. *J. Hydrometeor.,* **9,** 1073–1083.

Bosilovich, M. G., and S. D. Schubert, 2002: Water vapor tracers as diagnostics of the regional hydrologic cycle. *J. Hydrometeor.,* **3,** 149–165.

——, D. Mocko, J. O. Roads, and A. Ruane, 2009: A multimodel analysis for the Coordinated Enhanced Observing Period (CEOP). *J. Hydrometeor.,* **10,** 912–934.

Brubaker, K. L., D. Entekhabi, and P. S. Eagleson, 1993: Estimation of continental precipitation recycling. *J. Climate,* **6,** 1077–1089.

Castro, C. L., R. A. Pielke Sr., and J. O. Adegoke, 2007: Investigation of the summer climate of the contiguous United States and Mexico using the Regional Atmospheric Modeling System (RAMS). Part I: Model climatology (1950–2002). *J. Climate,* **20,** 3844–3865.

Collins, W. D., and Coauthors, 2006: The Community Climate System Model version 3 (CCSM3). *J. Climate,* **19,** 2122–2143.

Dirmeyer, P. A., 2006: The hydrologic feedback pathway for land–climate coupling. *J. Hydrometeor.,* **7,** 857–867.

——, C. A. Schlosser, and K. L. Brubaker, 2009: Precipitation, recycling, and land memory: An integrated analysis. *J. Hydrometeor.,* **10,** 278–288.

Dominguez, F., P. Kumar, X.-Z. Liang, and M. Ting, 2006: Impact of atmospheric moisture storage on precipitation recycling. *J. Climate,* **19,** 1513–1530.

Druyan, L. M., and R. D. Koster, 1989: Sources of Sahel precipitation for simulated drought and rainy seasons. *J. Climate,* **2,** 1438–1446.

Eltahir, E. A. B., and R. L. Bras, 1996: Precipitation recycling. *Rev. Geophys.,* **34,** 367–378.

Guo, Z., and Coauthors, 2006: GLACE: The Global Land–Atmosphere Coupling Experiment. Part II: Analysis. *J. Hydrometeor.,* **7,** 611–625.

Hagemann, S., K. Arpe, and L. Bengtsson, 2005: Validation of the hydrological cycle of ERA-40. ERA-40 Project Rep. Series 24, 46 pp. [Available online at http://www.ecmwf.int/publications/library/ecpublications/_pdf/era/era40/ERA40_PRS24.pdf.]

Kalnay, E., and Coauthors, 1996: The NCEP/NCAR 40-Year Reanalysis Project. *Bull. Amer. Meteor. Soc.,* **77,** 437–471.

Koster, R. D., and Coauthors, 2006: GLACE: The Global Land–Atmosphere Coupling Experiment. Part I: Overview. *J. Hydrometeor.,* **7,** 590–610.

Kurita, N., N. Yoshida, G. Inoue, and E. A. Chayanova, 2004: Modern isotope climatology of Russia: A first assessment. *J. Geophys. Res.,* **109,** D03102, doi:10.1029/2003JD003404.

Lawrence, D. M., P. E. Thornton, K. W. Oleson, and G. B. Bonan, 2007: The partitioning of evapotranspiration into transpiration, soil evaporation, and canopy evaporation in a GCM: Impacts on land–atmosphere interaction. *J. Hydrometeor.,* **8,** 862–880.

Lucarini, V., R. Danihlik, I. Kriegerova, and A. Speranza, 2007: Does the Danube exist? Versions of reality given by various regional climate models and climatological data sets. *J. Geophys. Res.,* **112,** D13103, doi:10.1029/2006JD008360.

Maurer, E. P., A. W. Wood, J. C. Adam, D. P. Lettenmaier, and B. Nijssen, 2002: A long-term hydrologically based data set of land surface fluxes and states for the conterminous United States. *J. Climate,* **15,** 3237–3251.

Mesinger, D., and Coauthors, 2006: North American Regional Reanalysis. *Bull. Amer. Meteor. Soc.,* **87,** 343–360.

Notaro, M., 2008: Statistical identification of global hot spots in soil moisture feedbacks among IPCC AR4 models. *J. Geophys. Res.,* **113,** D09101, doi:10.1029/2007JD009199.

Numaguti, A., 1999: Origin and recycling processes of precipitating water over the Eurasian continent: Experiments using an atmospheric general circulation model. *J. Geophys. Res.,* **104,** 1957–1972.

Roads, J., and Coauthors, 2003: GCIP water and energy budget synthesis (WEBS). *J. Geophys. Res.,* **108,** 8609, doi:10.1029/2002JD002583.

Ruane, A. C., and J. O. Roads, 2008: Dominant balances and exchanges of the atmospheric water cycle in the Reanalysis 2 at diurnal, annual, and intraseasonal time scales. *J. Climate,* **21,** 3951–3966.

Salvucci, G. D., J. A. Saleem, and R. Kaufmann, 2002: Investigating soil moisture feedbacks on precipitation with tests of Granger causality. *Adv. Water Resour.,* **25,** 1305–1312.

Seneviratne, S. I., D. Lüthi, M. Litschi, and C. Schär, 2006: Land-atmosphere coupling and climate change in Europe. *Nature,* **443,** 205–209.

Trenberth, K. E., 1999: Atmospheric moisture recycling: Role of advection and local evaporation. *J. Climate,* **12,** 1368–1381.

——, and C. J. Guillemot, 1998: Evaluation of the atmospheric moisture and hydrological cycle in the NCEP/NCAR reanalyses. *Climate Dyn.,* **14,** 213–231.

Uppala, S. M., and Coauthors, 2005: The ERA-40 Re-Analysis. *Quart. J. Roy. Meteor. Soc.,* **131,** 2961–3012, doi:10.1256/qj.04.176.

Wang, A. H., X. Zeng, S. S. P. Shen, Q.-C. Zeng, and R. E. Dickinson, 2006: Time scales of land surface hydrology. *J. Hydrometeor.,* **7,** 868–879.

Wang, G., Y. Kim, and D. Wang, 2007: Quantifying the strength of soil moisture–precipitation coupling and its sensitivity to changes in surface water budget. *J. Hydrometeor.,* **8,** 551–570.

Wei, J., R. E. Dickinson, and H. Chen, 2008: A negative soil moisture–precipitation relationship and its causes. *J. Hydrometeor.,* **9,** 1364–1376.

Zeng, X., 1999: The relationship between precipitation, cloud-top temperature, and precipitable water over the tropics. *J. Climate,* **12,** 2503–2514.

Zhang, C., 2005: Madden-Julian oscillation. *Rev. Geophys.,* **43,** 1–36.

Zhang, J., W.-C. Wang, and L. R. Leung, 2008: Contribution of land-atmosphere coupling to summer climate variability over the contiguous United States. *J. Geophys. Res.,* **113,** D22109, doi:10.1029/2008JD010136.